DOE/BC--92001062

Distributio DE92 001062

A Pore-Level Scenario for the Development of Mixed-Wettability in Oil Reservoirs

By
A. R. Kovscek
H. Wong
C. J. Radke

September 1992

Prepared for
U.S. Department of Energy
Assistant Secretary for Fossil Energy

Thomas B. Reid, Project Manager
Bartlesville Project Office
P. O. Box 1398
Bartlesville, OK 74005

Prepared by
Lawrence Berkeley Laboratory
University of California
Berkeley, California

Table of Contents

A Pore-Level Scenario for the Development of Mixed-Wettability in Oil Reservoirs

A. R. Kovscek, H. Wong, and C. J. Radke*
Earth Science Division of Lawrence Berkeley Laboratory
and Department of Chemical Engineering
University of California, Berkeley
Berkeley, CA 94720

* Author to whom correspondence should be addressed.

Abstract

Understanding the role of thin films in porous media is vital if wettability is to be elucidated at the pore level. The type and thickness of films coating pore walls determines reservoir wettability and whether or not reservoir rock can be altered from its initial state of wettability. Pore shape, especially pore wall curvature, is an important factor in determining wetting-film thicknesses. Yet, pore shape and the physics of thin wetting films are generally neglected in models of flow in porous rocks. This paper incorporates thin-film forces into a collection of star-shaped capillary tubes model to describe the geological development of mixed-wettability in reservoir rock. Here, mixed-wettability refers to continuous and distinct oil and water-wetting surfaces coexisting in the porous medium. The proposed model emphasizes the remarkable role of thin films.

New pore-level fluid configurations arise that are quite unexpected. For example, efficient water displacement of oil (i.e, low residual oil saturation) characteristic of mixed-wettability porous media is ascribed to interconnected oil lenses or rivulets which bridge the walls adjacent to a pore corner. Predicted residual oil saturations are approximately 35 % less in mixed-wet rock compared to completely water-wet rock. Calculated capillary pressure curves mimic those of mixed-wet porous

media in the primary drainage of water, imbibition of water, and secondary drainage modes. Amott-Harvey indices range from -0.18 to 0.36 also in good agreement with experimental values. (Morrow et al, 1986; Judhunandan and Morrow, 1991).

Introduction

The wettability of reservoir rock is a critical factor in determining the displacement effectiveness and ultimate oil recovery by drive fluids, such as water. Since the most wetting fluid tends to occupy the smallest and, hence, most hydrodynamically resistive pore channels while the least wetting fluid distributes to the largest and least resistive pore channels, wettability is a prime factor controlling multiphase flow and phase trapping. Therefore, understanding how wettability is established at the pore level is crucial if predictive flow models are to be developed.

Wettability in porous media is generally classified as either homogeneous or heterogeneous. For the homogeneous case the entire rock surface has a uniform molecular affinity for either water or oil. Conversely, heterogeneous wettability indicates distinct surface regions that exhibit different affinities for oil or water.

Three broad classifications of homogeneous wetting exist: strongly water-wet, strongly oil-wet, and intermediate-wet. If smooth representative rock surfaces can be prepared, then contact angles for water-wet surfaces, measured through the water phase, are near zero. Whereas, for oil-wet surfaces they are near 180°. In the case of intermediate-wetting, the rock has neither a strong affinity for water nor oil, and contact angles range roughly from 45° to 135° (Craig, 1971).

Two types of heterogeneous wettability are generally recognized. Mixed-wettability refers to distinct and separate water-wet and oil-wet surfaces which coexist and span a porous medium. Dalmation, also speckled or spotted, wettability refers to continuous water-wet surfaces enclosing regions of discontinuous oil-wet surfaces or vice-versa (Cuiec, 1991).

For many years, it was common petroleum-engineering practice to assume that oil reservoirs are strongly water-wet. Because most reservoir rock is highly siliceous and because oil reservoirs evolve by oil migrating into initially brine-occupied pore

space, it was thought that the rock surface maintains a strong affinity for water even in the presence of oil (Morrow, 1991). In 1973, however, Salathiel established that reservoirs with mixed-wettability display low residual oil (i.e., oil trapped as isolated globules) and consequently high displacement efficiency, as gauged by the ratio of oil recovered after waterflooding to the original oil in place. More recently, Fassi-Fihri et al (1991) use cryo-scanning electron microscopy to confirm that wettability is heterogeneous on the pore scale in actual reservoir media and that mineralogy greatly affects the type of wettability.

The purpose of this paper is to develop a pore-level picture of how mixed-wettability might form and evolve in reservoir rock initially filled with brine. Before embarking on this task we briefly review the characteristics of mixed-wettability as observed by Salathiel (1973).

Mixed-Wettability

Following standard protocol, Salathiel oilflooded cores that were initially filled with brine until little or no water was produced. This simulates the original migration of oil into an oil- bearing reservoir rock. The water saturation following completion of oil migration is commonly referred to as connate saturation.

Next the core was waterflooded until little or no more oil eluted. If no further oil can be produced, this saturation is known as residual or irreducible. Prior to achieving residual oil saturation, oil which may still be displaced is called remaining oil. When using an asphaltic East-Texas crude oil with either actual reservoir core or Boise sandstone, Salathiel found residual oil saturations of less than 10 %. Small amounts of oil continued to be produced even after thousands of waterflood pore volumes.

This result is quite opposite to that usually encountered. Indeed, when n-heptane or a viscous white oil replaced the crude oil, Salathiel established residual oil

saturations near the commonly observed values of 25 to 40 % within several waterflood pore volumes. Fascinatingly, when a small volume of the asphaltic crude was diluted into the n-heptane, the waterflood performance was essentially the same as that of the original reservoir crude oil. Further, for the asphaltene-laden oils, lower initial connate water saturation correlated with lower residual oil content. Oilflooding a previously waterflooded core led to irreducible water saturations much higher than the initial connate value.

Salathiel's explanation of his experimental results is pictured in Figure 1. This figure shows proposed pore-level configurations of oil and water after extensive waterflooding of an asphaltic oil. Water flows into the plane of the drawing. Near the cusps of the grain contacts, the rock is protected from the effects of the asphaltic oil and remains water wet. On the central portion of each grain surface away from the cusps, an oil-wet surface is created due to the deposition of asphaltic components of the crude oil. The continuous oil-wet paths, which span from pore to pore, allow oil to be swept along the rock surface almost indefinitely by the viscous traction of flooding water. Oil trapping is thereby obviated, but production rates are small.

As wettability is molecular in origin, a succinct description of mixed-wettability follows from considering the effects of thin films which coat and adhere to solid surfaces. Thin-film forces in fact control wettability. Before discussing the geological evolution of mixed-wettability, it is necessary to explore the relationship between thin films and wettability.

Thin Films and Wettability

Figure 2 displays a schematic of an apparatus used to quantify thin-film forces in liquid films adjacent to a solid surface (Derjaguin et al, 1978). An annular porous disk, which allows flow of wetting fluid, is sealed against a solid substrate. A

nonwetting fluid meniscus enters from below the solid substrate disk assembly. Far away from the solid substrate, the meniscus is hemispherical. When the central portion of the meniscus is pressed against the wall, a thin film forms. As the pressure of the nonwetting fluid rises compared to that in the wetting fluid, the film thins and the meniscus or Plateau border recedes into the corner. An experiment proceeds by applying a capillary pressure difference (i.e., $P_c = P_{nw} - P_w$) across the Plateau-border meniscus and measuring the resulting thickness of the film by interferometry or ellipsometry.

At equilibrium, the pressure of the wetting fluid in the thin film and the Plateau border are identical. The film is flat, yet the capillary pressure is nonzero. Consequently, the standard Young-Laplace equation of capillarity does not describe the thin film portion of Figure 2. Rather, thin-film forces must be incorporated into the Young-Laplace equation by adding a term, $\Pi(h)$, referred to as disjoining pressure (Derjaguin and Obukhov, 1936; Derjaguin and Kussakov,1939a, 1939b; Derjaguin et al, 1987):

$$P_c = \sigma\left(\frac{1}{r_1} + \frac{1}{r_2}\right) + \Pi(h) \; . \qquad (1)$$

In the augmented Young-Laplace equation, σ refers to the bulk interfacial tension between the wetting and nonwetting phases for an interface with principal radii of curvature r_1 and r_2.

Disjoining pressure is a function of film thickness, h. If disjoining pressure is positive, the two interfaces repel each other, whereas if disjoining pressure is negative the two interface attract. When films are thin (e.g., 100 nm), the disjoining pressure is significant compared to the other terms in Eq. 1. For the flat film in Figure 2 the curvature is zero so that at equilibrium $P_c = \Pi(h)$. Equation 1 may be cast in

dimensionless form by a characteristic force, σ, and a characteristic dimension, a_m. Representative values σ and a_m are 50 mN/m and 150 μm, respectively. With this scaling the first term on the right side of Eq. 1 varies from approximately 1/3 to 10, whereas a disjoining pressure of 500 Pa makes the second term of order 1.

A schematic disjoining pressure isotherm is drawn in Figure 3. For certain values of disjoining pressure, for example Π_1, there are three possible equilibrium film thicknesses. The outermost films have thicknesses of order 10 to 100 nm. The central portion of the Π versus h curve (i.e., where $d\Pi/dh$ is positive) is an unstable region (Chambers and Radke, 1991). A film in this thickness region spontaneously thickens or thins to a new stable configuration. The innermost films are quite thin, possibly on the order of one or several monolayers of solvent molecules. The effective range of the disjoining pressure is denoted by h_p.

Many factors contribute to the shape of a disjoining pressure isotherm. Three major force components are electrostatic interactions, van der Waals interactions, and hydration forces (Melrose, 1982). The first, electrostatic forces, originate from the overlap of ionic clouds present at each interface known as electrical double layers. For symmetric charged films, these are repulsive stabilizing forces (Callaghan and Baldry, 1978). Melrose (1982) and Hall et al (1983) give thorough discussions of double-layer repulsive forces and their effects on film stability. Dispersive van der Waals forces are usually attractive and destabilize thin-aqueous films (Melrose, 1982). Lastly, strong repulsive hydration forces are important at film thicknesses approaching molecular dimensions (Hirasaki, 1991).

Clearly, the mineral content of pore walls has a large effect on thin-film interaction forces. For example, when a drop of crude oil is contacted with a brine-covered surface, crude oil adheres more readily (i.e., thick aqueous films break more easily) on calcite than quartz (Morrow, 1990). Because calcite has a more positive

surface charge, under identical conditions there is less stabilizing repulsive action from the electrostatic overlap forces.

Oil-drop adhesion tests provide a simple approach to characterize the wetting behavior of crude oils against solid surfaces (Morrow et al, 1986; Buckley et al, 1989; Buckley and Morrow, 1990). When adhesion occurs, it is found that the solid/oil/water boundary is fixed or "pinned" at the three-phase contact line (Morrow, 1990). Accordingly, the contact line of a retracting oil drop does not recede along the solid substrate. In subsequent sections, the importance of contact-angle pinning in mixed-wettability systems will be evident.

Thin-film forces determine the contact angle, the most widely used measure of wettability. Direct integration of the augmented Young-Laplace equation yields the following relationship between equilibrium contact angle, θ, and disjoining pressure (Wong et al, 1992),

$$\cos\theta - 1 = \frac{1}{\sigma}\left[\int_h^{h_p} \Pi(\xi)d\xi - (h_p - h)\Pi(h)\right] . \qquad (2)$$

In Eq. 2 h is the equilibrium film thickness of interest. Implicit in Eq. 2 is the constraint that $h_p/a_m << 1$.

Integration over the positive purely repulsive portions of Figure 3 (i.e., the thick outer films) results in zero contact angle. Conversely, nonzero contact angles up to 90° are possible when Eq. 2 is integrated over the attractive negative portions of Figure 3 (Wong et al, 1992). The above equation is derived for a meniscus attached to a flat solid surface. Nevertheless, it still applies for solid curved surfaces as long as the film thickness is much smaller than the radius of curvature of the surface.

Consider now films on significantly curved surfaces. Figure 4 displays one such surface: two spherical solid beads with diameters d_1 and d_2 covered with a layer of

wetting fluid. The curvature of the films is nonzero and the curvature term on the right side of Eq. 1 now contributes. If the wetting films are convex, as in Figure 4, the curvature of the interface is deemed negative.

Assume now that the films in Figure 4 are under an imposed capillary pressure and that the films are thin enough so that the curvature of the film far away from the bead contact is roughly that of the bead (i.e., $h_i/d_i << 1$). In this situation, the smaller the bead diameter the more negative is the film curvature. Rearranging Eq. 1 and invoking the geometry of Figure 4 we write that

$$\Pi(h_i) = P_c + \frac{4\sigma}{d_i} \quad . \tag{3}$$

Thus to maintain equilibrium with a fixed capillary pressure, the film disjoining pressure must rise as the diameter, d_i, of a bead decreases. Accordingly, the thin film coating the smaller bead is thinner than that coating the larger bead. The second term on the right side of Eq. 3 contributes 2000 Pa when d_i is 100 μm and σ is 50 mN/m.

According to Figure 3, film thickness decreases monotonically with increased capillary pressure until the local maximum in disjoining pressure, Π^{max}, is reached. This corresponds to a critical capillary pressure, P_c^*, for thick-film rupture. When the capillary pressure exceeds P_c^*, the thick outer film sheets away and only a molecularly adsorbed film resides next to the surface. Because the disjoining pressure is largest in the film coating the smallest bead, that film becomes unstable first and consequently exhibits the smallest P_c^*. Inserting Π^{max} into Eq. 3 gives P_c^* for any bead diameter. Equation 2 teaches that exceeding the critical capillary pressure also signals a transition in the contact angle. Our discussion so far is quite general and applies to oil films between a solid and brine as well as aqueous films between a solid

and oil. Next, we discuss one manner in which a water-wet surface transforms into an oil-wet surface.

When a thick aqueous wetting film collapses into a molecularly thin one, surface active components from asphaltic oil can, in some instances, adsorb irreversibly onto the surface. Asphaltenes (i.e., high molecular weight aggregates insoluble in light normal alkanes but soluble in benzene or pyridine) occur in relatively large quantities in many crude oils. It is currently believed that asphaltenes are colloidal polydispersions comprised of flat, disklike aggregates (Dubey and Waxman, 1991). They are usually coated with lower molecular weight resins (Chung et al, 1991). Resins adsorbed to the asphaltene surfaces apparently stabilize the asphaltene colloidal dispersions .

Clementz (1976, 1982) demonstrated that the heavy ends fraction of crude oil (i.e., asphaltenes) adsorbs strongly to clay materials at low water content. Also, Dubey and Waxman (1991) showed that asphaltenes adsorb quite readily to clay materials in the absence of both brine and resins. The asphaltene aggregates apparently adsorb with their disk faces against the planar faces of the clay. Asphaltene adsorption appears irreversible for all practical purposes (Morrow et al, 1986; Hirasaki et al, 1990; Dubey and Waxman, 1991). Strong solvents and extensive cleaning procedures are necessary to desorb asphaltenes and resins. The key factor in asphaltene adsorption appears to be direct access of the asphaltic components of the oil to the rock surface without an intervening thick layer of water in which they are highly insoluble. Thus when the critical capillary pressure is exceeded, asphaltenes may adsorb because only a molecular aqueous film protects the solid surface.

In practice, surfaces within porous reservoir rock are curved and rough. Hence, it is difficult to measure contact angles and to determine directly the extent of connectivity of water and oil-wetting surfaces. Fortunately, capillary pressure as a function of water saturation exhibits characteristic shapes for different types of

wettability in porous media. Morrow (1990) and Cuiec (1991) review how wettability may be assessed from experimental capillary-pressure information.

Figure 5 contrasts typical experimental capillary pressure curves for water-wet (Figure 5a) and mixed-wet rock (Figure 5b). Measurement of capillary pressure usually begins with the porous rock sample saturated with the wetting phase. Under the action of, for example, a centrifuge (Slobod, 1951) nonwetting fluid is driven into the sample causing an increase in capillary pressure and primary drainage of the wetting phase. Large capillary pressures leading to low wetting phase saturations are obtained at high rotational speeds. When the applied capillary pressure is then lessened incrementally, the porous sample spontaneously imbibes the wetting phase thereby displacing nonwetting fluid. Equilibrium capillary-pressure measurements are made possible in this fashion. Spontaneous imbibition continues until the interfacial curvature reaches zero. For the mixed-wettability rock, additional wetting phase imbibes under applied (centrifugal) pressure. Hence, the wetting-phase pressure exceeds that of the nonwetting phase and negative capillary pressures occur, as illustrated in Figure 5b. Strongly water-wetting rock does not display negative capillary pressures under forced imbibition. Finally, secondary drainage of water follows imbibition.

Hysteresis is evident in the curves shown in Figure 5. The wetting phase drains from the largest pores first causing relatively large changes in saturation with moderate changes in capillary pressure. Conversely, wetting phase imbibes into the smallest pore spaces first because of capillary suction. This causes large changes in capillary pressure with only moderate changes in saturation.

The extent of imbibition and drainage processes define empirical wettability indices (Morrow, 1990; Cuiec, 1991). One such index is the Amott-Harvey index, I_{wo}. This index ranges from +1 for strongly water-wetting rock to -1 for strongly oil-wetting rock. A value of zero indicates neither strong water nor strong oil wettability. Thus, the

I_{wo} for the water-wet rock in Figure 5a is 1, while the weakly mixed-wet rock of Figure 5b has an I_{wo} of -0.05. Further discussion of wettability indices and their significance is deferred until later.

Geological evolution of mixed-wettability is described by following pore-level events through the cycle of primary drainage, spontaneous imbibition, forced imbibition, and secondary drainage. Asphaltene adsorption onto solid surfaces is allowed if thick protective water films break. Immediately following the outline of pore-level events, theoretical capillary pressure curves are calculated to gauge the extent of oil-wettability via Amott-Harvey indices.

Theory

Initially, reservoir rock is saturated with brine (the terms brine and water are used interchangeably) and strongly water-wetting. Reservoir rock unaltered from its original state is referred to as pristine. Actual pores in reservoir media are lined by nooks or axial grooves (Chambers and Radke, 1991). Accordingly, the porous medium is modeled as a collection of star-shaped translationally invariant pores, as illustrated in Figure 6. The star shape is chosen because it is nonaxisymmetric, cornered, and resembles the open area between 4 rods or 4 sand grains in cross section when they are in contact. The radius of the largest circle which can be inscribed in a pore is denoted as a. We adopt such a simple model of a porous medium to emphasize the fascinating role of thin films on wettability. Because reservoir-scale flow rates and gravitational forces are small, all continuous, immiscible phases are separated by constant curvature surfaces in capillary equilibrium. End effects are not considered. Capillary pressure is consistently defined as the oil-phase pressure minus the aqueous-phase pressure.

Single-Pore Events

We begin with a single brine-filled star-shaped pore of size a that is initially strongly water-wet and consider pore-level events as a function of changing capillary pressure. Later we incorporate a pore-size distribution and generate capillary pressure curves. Oil cannot invade into the single pore until the capillary entry pressure, P_c^e, is exceeded. This initial drainage of brine is called pristine drainage. For a star-shaped pore with zero contact angle, the capillary entry pressure is given by (Mayer and Stowe, 1965)

$$\frac{aP_c^e}{\sigma} = 1.86 \quad . \tag{4}$$

For $P_c \geq P_c^e$ oil enters the tube with a constant meniscus curvature displacing brine from the central portion of the tube leaving brine only in the corners, as illustrated in Figure 7. Light shading represents brine while dark shading represents oil. Thick aqueous films lie between the solid pore walls and the oil. Their thickness is determined by the capillary pressure and the form of the disjoining pressure isotherm (c.f., Figure 3). The configuration of the brine-filled corners away from the invading meniscus is that of constant curvature circular arcs.

The curvature of the so-called arc menisci (Morrow and Mason, 1991) does not change until the invading meniscus empties the entire middle portion of the tube. After which, the arc menisci increase their curvature in response to higher imposed capillary pressures and advance toward the cusp. Thus, as more oil enters the tube, the capillary pressure climbs, the aqueous films coating pore walls thin, and the disjoining pressure climbs.

At the critical capillary pressure, P_c^*, for this sized pore, the thick films become unstable and spontaneously thin to molecularly adsorbed films. Since h/a << 1, the thick films coating the walls of star-shaped pores have approximately the same curvature as the pore walls. Consequently, the critical capillary pressure for thick wetting-film collapse is

$$P_c^* = \Pi^{max} - (\sqrt{2} - 1)/a \quad . \qquad (5)$$

The second term on the right incorporates the curvature of the film adhering to the pore wall. It is negative (because the pore wall is convex) causing P_c^* to be less than Π^{max}, the primary maximum in disjoining pressure (c.f. Figure 3). For smaller pore sizes P_c^* is smaller and vice versa. Hence, P_c^* may not be attained in all pores. The drainage and film-breakage processes continue as the capillary pressure is increased to a maximum, P_c^{max}.

In accordance with Eq. 2, the ultrathin molecular films, produced for $P_c > P_c^*$, do not exhibit the same contact angle as that for thick wetting films. Disjoining pressure isotherms have not been measured for solid/water/oil systems of interest. Therefore, we approximate contact angles for the molecular aqueous films as 20° rather than calculate specific contact angles for each film thickness. The contact angle is 0° for the thick films (i.e., $P_c^{max} < P_c^*$) since they lie on the purely repulsive portion of the disjoining pressure curve.

When P_c^{max} is quite large, the brine content of the pore in Figure 7 is very low. Oil reservoirs remain at low water saturations for geological periods of time. We assert that asphaltenes adsorb along the walls of the oil-occupied pores where thick protective water films are broken (i.e., those pores for which $P_c^{max} > P_c^*$). The location

along pore-walls where asphaltenes adsorb is displayed schematically in Figure 8 as a white region recessed from the pore wall.

No asphaltene adsorption occurs within larger pores for which $P_c^* > P_c^{max}$ because thick protective water films coat pore surfaces. We designate this type of pore as water-wet. Because asphaltenes are insoluble in water, it is apparently not possible for them to dissolve in and transport across the thick water films to contact the pore walls. However, the resin-coated asphaltene aggregates are much larger than the molecular dimensions of water. Hence, they can, over time, span the molecular layers of water coating smaller oil-occupied pores in which $P_c^* < P_c^{max}$ causing some water molecules to desorb, and, thus, directly contact the rock surface to adsorb irreversibly. Salathiel (1973) observed such asphaltene adsorption on sandstones within hours. It is not clear whether the resins coating the asphaltene colloids or the asphaltene aggregates themselves actually bind to the surface in the presence of molecular water films.

Figure 8 also illustrates that there are two distinct regions of wettability in pores where asphaltenes adsorb. A step change in wettability exists at the contact line between the asphaltene-coated portion of the pore wall and the water-filled corner. This contact line is pinned at the position it established at P_c^{max} . The corners of the pore retain bulk water preventing asphaltene adsorption and, thus, preserving their water-wettability. Away from pore corners, the highly hydrophobic adsorbed asphaltenes make that portion of the pore wall oil-wet. We designate this type of pore as mixed-oil-wet.

In mixed-oil-wet pores the three-phase contact line is pinned and does not move in response to variation in capillary pressure. Instead, resulting curvature changes are accommodated at the pinned water/oil interface by changes the angle of the contact line. This pinned angle of contact is free to assume values between 20° and 180°.

Following adsorption of asphaltenes, the course of pore-level events through imbibition and secondary-drainage processes differs radically between a mixed-oil-wet and a water-wet pore. Each is discussed below.

Water-Wet Pore

Upon imbibition, the water-wet pore immediately refills with water. The menisci here are not pinned and thus follow the exact reverse of pristine drainage in response to a decreasing applied capillary pressure. As the capillary pressure falls, the menisci move away from the pore corners at zero equilibrium contact angle. This continues until the menisci touch to form an inscribed circle (see Figure 9). However, the inscribed circle configuration is unstable (Ransohoff et al, 1987) in that any infinitesmal disturbance in the streamwise direction must grow. As first described by Roof (1970), the oil snaps off in order to achieve a minimum energy configuration.

Morrow and Mason (1991) argue that for perfectly wetting triangular pores, the resulting disconnected cylinders of oil created by snap-off exhibit curvatures corresponding to the entry curvature. We adopt the same reasoning here and demand that the curvature of the snapped-off oil drop be that given by Eq. 4. Snapped-off oil is distributed along the length of the water-wet pores as isolated cylinders of oil resembling sausages with hemispherical-like end caps and curvatures corresponding to the appropriate entry curvature. The length of the isolated oil cylinders is determined by long wavelength disturbances which cause breakup of the oil column, roughly $2\pi a$ (Chambers and Radke, 1991).

After snap-off, the isolated oil sausages are disconnected from the continuous oil fraction and are no longer under the influence of the applied capillary pressure. In our equilibrium scenario, there is no facility to displace this discontinuous oil. Even if small pressure gradients are imposed, the disconnected oil eventually encounters a pore constriction and traps. Therefore, snapped-off oil is termed here residual oil.

The fluid configuration in the water-wet pore remains unchanged until secondary drainage of water occurs. At the appropriate entry pressure for this sized pore, oil enters the water-wet pore, as during pristine drainage, and reconnects with the residual oil already present. Once the central portion of the pore refills with oil (c.f., Figure 7), the arc menisci again move toward the pore corner as the capillary pressure climbs. Upon completion of secondary drainage, the water-wet pore contains continuous oil in the center of the pore and continuous brine in the corners connected to thick continuous water films along the pore walls in an exact replica of pristine drainage.

Mixed-Oil-Wet Pore

Figures 10 and 11 display pertinent events in a mixed-oil-wet pore (i.e., one in which $P_c^{max} > P_c^*$ so that molecularly adsorbed water films coat the pore walls away from the corners) as it proceeds through imbibition and secondary-drainage processes. Recall that the three-phase contact line in a mixed-oil-wet pore is pinned at the location it attained at P_c^{max}. Upon gradual lowering of the imposed capillary pressure, water imbibes spontaneously due to capillary suction until the curvature of the pinned water-oil interfaces falls to zero (Figure 10a). At zero imposed capillary pressure the mixed-oil-wet pore contains continuous oil in the center and continuous brine in the corners with an interfacial curvature of zero.

Further imbibition into the mixed-oil-wet pore occurs when water is forced into the rock. Water-phase pressure now exceeds oil-phase pressure. Hence, negative capillary pressures arise, and this process is referred to as forced imbibition. Because the fraction of water-wet surfaces in a mixed-oil-wet pore is quite small, the pore appears completely oil-wet (i.e., a contact angle of 180° measured through the water phase) to the water-invasion process. Thus, forced water invasion is directly analogous to forced oil entry into completely water-wet pores (i.e., a contact angle of

zero). Accordingly, the entry curvature of the eight-fold symmetric star-shaped pore is given by

$$\frac{aP_c^e}{\sigma} = -1.86 \ , \qquad (6)$$

where the negative sign arises because of the 180° contact angle (c.f., Eq. 4).

Figure 10b displays the oil and water configurations in the mixed-oil-wet pore just after water invasion. A thick lens or rivulet of oil bridges the corner of the pore separating brine in the pore center from that in the pore corner. This bridging, oil-lens configuration is readily argued to be stable (Ransohoff et al, 1987). An oil film coats the central portion of the pore wall. The original three-phase contact line nearest the corner remains pinned while the newly created meniscus establishes an equilibrium contact angle against the pore wall.

Since asphaltene adsorption is virtually irreversible (Morrow et al, 1986; Hirasaki et al, 1990; Dubey and Waxman, 1991), we postulate that all thicknesses of oil films deposited on asphaltene-coated surfaces are stable. It follows that the oil-film disjoining pressure is purely repulsive. Thus, the solid surface is completely wetted by oil, and the newly created meniscus establishes a contact angle of 180° measured through the water phase. If measured through the oil phase, the contact angle is zero reflecting a monotonic repulsive disjoining pressure isotherm and Eq. 2. More structure to the oil-film disjoining pressure isotherm is possible (Hirasaki, 1991), but leads to no significant differences in overall pore-occupancy configurations.

Oil contained in the lenses of Figure 10b is translationally continuous. Consequently, all of the oil drains, although slowly, as the capillary pressure becomes more negative. When the lenses are nearly empty of oil, the two water/oil interfaces composing each lens meet.

Two possibilities exist for the behavior of the oil lenses when the water/oil interfaces touch. In case 1 the lens is unstable and breaks. The small amount of oil contained in the lens when it breaks flows via the continuous oil-wet surfaces to surrounding pores. In case 2 a stable thin water-in-oil (W/O) emulsion film is created which bridges the pore corners. A repulsive, stabilizing disjoining pressure in the thin water/oil/water film is required for case 2. We assume here that any W/O emulsion films are stable within the range of applied capillary pressures. If the W/O emulsion films are not stable over the range of capillary pressures applied, case 1 is recovered. Regardless of which picture is adopted, the mixed-oil-wet pore becomes completely filled with water except for a small oil fraction that exists as either thin oil films along the solid surface of the pore or as W/O emulsion films which span each pore corner and which are connected to thin oil films lying along the solid pore surface.

Pore-level events differ significantly for cases 1 and 2 during secondary drainage of water. In the case of unstable lenses, beginning at the minimum negative imposed capillary pressure, the oil films lining the walls of the mixed-oil-wet pore thicken following Eq. 1. The oil resides as thin films until the capillary pressure is positive and exceeds the magnitude of the wall curvature (i.e., $P_c \geq (\sqrt{2} - 1)/a$).

Upon increasing the positive capillary pressure further, oil invades along the pore walls, as shown in Figure 11a. Pinning is still demanded at the step change in wettability on the pore surface. Once the expanding oil interfaces touch, an unstable fluid configuration again arises. The brine in the very center of the pore rearranges into cylindrical droplets with rounded end caps which span the pore. In cross-section, these fluid configurations are very similar to those displayed in Figure 10b for forced imbibition except that the outermost pinned oil/water interfaces bow toward the corners. Oil maintains continuity along the length of the pore, but the brine in the center of the pore is no longer continuous. Individual discontinuous brine droplets are separated axially by thick oil bridges perpendicular to pore walls and connected to the

oil lenses running the length of the pore. This discontinuous brine is the direct analogue to discontinuous trapped oil and is referred to as irreducible water. Mixed-oil-wet pores are requisite to producing irreducible trapped water. In strongly water-wet porous media there is no irreducible water. Rather, connate water in the pore corners is continuous, and the connate saturation simply decreases as the imposed capillary pressure rises (c.f., Figure 7).

In the case of stable W/O emulsion films (i.e., case 2), oil refills the thin oil films bridging the corners of the pore beginning at P_c^{min}, as illustrated in Figure 11b. The free oil meniscus (i.e., the inner most one which is unpinned) grows at 180° contact angle while the outermost water/oil interface remains pinned at the contact line for the step change in wettability. Once the unstable inscribed circle configuration is attained (see Figure 11b), snap-off ensues, and the water disconnects giving rise to irreducible trapped water. The shape of the isolated cylinders of irreducible water is quite identical to that for case 1 except that the isolated water cylinders are separated axially by smaller oil bridges.

At the completion of secondary drainage for either case 1 or 2, the mixed-oil-wet pore contains continuous brine in the corners of the pore, continuous oil lenses, and disconnected irreducible brine in the center of the pores. If W/O emulsion films do not form (i.e., unstable lenses), irreducible brine is formed while the capillary pressure is positive during secondary drainage. If W/O emulsion films are stable within the range of applied capillary pressure, then irreducible brine is formed while capillary pressures are negative.

Results

The above series of pore-level fluid configurations leads directly to calculation of capillary pressure versus aqueous phase saturation curves once a distribution of pore sizes is specified. Figure 12 shows on a semi-logarithmic scale the discrete size distribution of star-shaped pores employed here. The distribution is nondimensionalized by the mean of the distribution, a_m, chosen as 150 μm. This particular distribution approximates roughly that found by Wardlaw et al (1987) for pores in a Berea sandstone. In addition to pore bodies, the adopted distribution also contains a significant number of pores which are exceptionally small. These represent pore throats and micropores. The frequency scale indicates the actual number of pores of a particular size used in the calculations to follow.

Capillary pressures are imposed by incrementing interfacial curvature, pore-level reconfiguration of fluids is assesed, and the saturation is calculated from a knowledge of interfacial curvature and fluid configuration. The known phase configurations lead directly to the aqueous phase saturation, $S_w = A_w/A_t$, where A_w is the cross-sectional area of the pores occupied by water and A_t is the total cross-sectional area of the pores. Once generated, the theoretical P_c versus S_w curves may be compared to typical experimental data. Numerical and geometrical details of the calculation are available elsewhere (Kovscek, 1992).

Capillary Pressure Curves

Figure 13 depicts capillary pressure versus aqueous phase saturation for case 1, unstable lenses. Pristine drainage occurs between the points labelled A through C. No oil enters the porous medium until point A where the capillary entry pressure is exceeded for the largest-sized pore. Each particular pore size has a unique entry pressure determined by Eq. 4 with the fluid configuration after entry shown in Figure 7. As the capillary pressure climbs oil flows into the porous medium, more capillaries are

entered, and the water saturation declines. The smallest-sized pores are not entered by oil because their capillary entry pressure is not exceeded. Consequently, they remain brine filled. The curve displayed in Figure 13 is not smooth because a discrete rather than smooth distribution of pore sizes is employed (c.f. Figure 12).

Following Eq. 5, each sized pore in the size distribution of has a unique critical capillary pressure for thick film stability. Films are thinnest along pore walls with the most negative curvature (i.e., those pore walls with the smallest radii of curvature). Thick protective films correspondingly break first in the smallest oil-occupied pores.

The area near point B on Figure 13 denotes the region where thick protective water films coating walls of intermediate-sized pores break. Larger pores do not exceed their particular P_c^* and thus remain water-wet. The drainage and thick film-breakage processes continue to P_c^{max}, the highest imposed capillary pressure (point C on Figure 13). Water saturation at this point is connate saturation, S_{wc}. Figure 7 reveals that large capillary pressures, such as P_c^{max}, correspond to low connate water saturation. This is consistent with Salathiel's (1973) original observations. It is possible to reduce water saturation further by exceeding P_c^{max}, because both phases maintain continuity throughout the pore structure. That is, no water is trapped at connate saturation in Figure 13.

Asphaltene adsorption also occurs at point C in those intermediate-sized pores which lack thick water films. After asphaltene adsorption, the smallest pores which were never entered by oil are completely brine filled. The intermediate-sized pores, which exceeded their critical capillary pressure for thick film stability, P_c^*, have asphaltenes adsorbed on the exposed rock surface and, hence, are mixed-oil-wet with a pinned contact line between the oil and water-wet regions. The largest pores, which did not exceed their corresponding P_c^*, remain water wet.

Upon a controlled decrease in capillary pressure, spontaneous imbibition commences between the points labelled C through E, and all pores refill with water (as

illustrated by Figures 9 and 10a). The water-wet and mixed-oil-wet pores follow individual imbibition paths. Near the point labelled D oil snaps off and traps in the water-wet pores. As the capillary pressure approaches zero, the large water-wet pores are filled with residual oil and no longer change saturation in response to capillary pressure changes. Further examination of Figure 10a teaches that small changes in the brine saturation of mixed-oil-wet pores cause large changes in interfacial curvature and, accordingly, large changes in capillary pressure. This explains the near step change in P_c in the vicinity of point E on Figure 13.

Forced imbibition at negative capillary pressures occurs along points E through G of Figure 13. Saturation changes occur only in the mixed-oil-wet pores because, as noted above, the smallest pores are completely brine filled and the largest pores are filled with trapped oil. Water imbibes into progressively smaller mixed-oil-wet pores as the capillary pressure becomes more negative (e.g., point F on Figure 13), and oil slowly drains from the bridging lenses or rivulets. As capillary pressure is made increasingly negative and decreases to P_c^{min} (point G of Figure 13), the oil saturation of the porous medium decreases to S_{or}, the residual oil saturation.

Secondary drainage for case 1, or unstable lenses, is denoted by points G through K. Beginning at point G, the oil films coating pore walls thicken, but the capillary pressure must be positive and exceed the magnitude of the pore wall curvature before significant amounts of oil can reinvade the mixed-oil-wet pores. Correspondingly, the capillary pressure rises sharply from point G to point H with little alteration in saturation. Oil then reoccupies the mixed-oil-wet pores, as illustrated in Figure 11a. Water traps near point I and leads to irreducible water saturation. With P_c now positive oil reenters the water-wet pores at the appropriate P_c^e (point J), as it did during pristine drainage. Oil filling continues until P_c^{max} is reattained at point K with saturation S_{wirr}. When another cycle of imbibition and drainage beginning from P_c^{max}

is made, a scanning or hysteresis loop is found between points K and G. A dashed line on Figure 13 illustrates how the scanning loop connects.

The pore-level events which distinguish case 1 from case 2 happen strictly during secondary drainage. Hence, the capillary pressure curve for case 2 differs from case 1 only during secondary drainage. On Figure 14 secondary drainage for case 2 is marked by the points G through P. Point G of Figure 14, the minimum imposed capillary pressure, is identical with point G of Figure 13.

Large volumes of oil, relative to case 1, immediately reinvade the stable W/O films at P_c^{min} during secondary drainage for case 2. Irreducible water is created at negative capillary pressures as marked by region M in Figure 14, consistent with the secondary-drainage mechanism illustrated in Figure 11b. Once snap off and trapping complete in the mixed-oil-wet pores, the applied capillary pressure rises quite rapidly with little change in saturation in the region around point N on Figure 14. The only saturation change in response to increasing capillary pressure occurs in the mixed-oil-wet pores at the pinned contact line, much as it did at point E on Figure 13 during spontaneous imbibition. With capillary pressures now positive, oil enters the water wet pores, for instance, at point O on Figure 14. Again the capillary pressure increases to P_c^{max}, point P on Figure 14. Similar to case 1, a scanning or hysteresis loop is found, now between points P and G, when the imbibition and drainage processes are repeated .

The theoretical capillary pressure curves compare quite favorably to experimental data for mixed-wet porous media. For instance, refer to Figure 5b, and the measurements of Sharma and Wunderlich (1987), and Hirasaki et al (1990). Further, the theoretical curves can now be evaluated to gauge the wettability of the porous medium. Amott-Harvey indices are the requisite tool.

Porous-Medium Wettability

Amott-Harvey indices are based on the saturation changes associated with spontaneous imbibition, ΔS_{ws}, secondary drainage, ΔS_{os}, and the overall saturation change during imbibition, ΔS_{wt} (Amott, 1959; Morrow, 1990). These quantities are defined on Figure 5b. First, the wettability index to water, $I_w = \Delta S_{ws}/\Delta S_{wt}$, is established as the ratio of spontaneous and overall saturation changes during imbibition. Next, the wettability index to oil, $I_o = \Delta S_{os}/\Delta S_{wt}$, is found from the ratio of saturation change during secondary drainage to the overall saturation change during imbibition. The difference between water and oil wettability indices, $I_{wo} = I_w - I_o$, is the Amott-Harvey index.

Amott-Harvey indices and residual oil saturation are presented in Table 1 for both mixed-wet cases on Figures 13 and 14 and for a water-wet case. Case 3, the water-wet example, has a nondimensional disjoining pressure maximum ($a_m\Pi^{max}/\sigma$), for aqueous films coating solid surfaces, that is 10 times larger than the mixed-wettability cases . This ensures that none of the thick water films coating pore walls rupture to molecularly adsorbed films within the range of applied capillary pressures. Asphaltene adsorption is thereby prohibited. Consequently, this case exhibits an I_{wo} of 1, as expected for strongly water-wetting rock. The Amott-Harvey index for W/O emulsion films (case 2) is less than that for unstable lenses (case 1). Since W/O emulsion films refill immediately with oil while capillary pressure is negative during secondary drainage, ΔS_{os} and I_o are significant for case 2. Accordingly, I_{wo} is smaller.

The unstable lenses and the stable W/O emulsion films exhibit identical residual oil saturations because in each case an identical amount of oil is contained in lenses, such as those shown in Figure 10b. Recovery of oil from these lenses is eventually complete. Pore-level events which change pore occupancy only differ after P_c^{min} and S_{or} are attained.

Relative to the water-wet case, residual oil saturation for the mixed-wet cases is much reduced. This is consistent with experimental observations (Salathiel, 1973; Jadhunandan and Morrow, 1991). However, the magnitude of S_{or} obtained experimentally is much lower than that predicted here. Our scenario over estimates residual oil primarily because the pores are not explicitly interconnected. In actual porous media, the connectivity or topology of the pore space strongly influences the displacement and entrapment of oil (Mohanty et al, 1987). It is well known that a network of pores with multiple connections allows more escape routes for oil to remain continuous.

Salathiel (1973) originally attributed extended oil recovery from mixed-wettability rocks to thin continuous oil films along the rock surface which allow almost indefinite oil displacement. In the scenario proposed here, we predict that most remaining oil occurs as lenses or rivulets which span the corners of mixed-oil-wet pores (c.f., Figure 10b). The oil films coating the oil-wet fraction of the pore walls allow surface drainage of oil, but the oil volumes they contribute is much less than that associated with lens drainage.

Figures 13 and 14 show that consistent with Salathiel's observations, connate and irreducible water saturations are not equal. This is a result of the wettability alteration that occurs at P_c^{max} during primary drainage. Oil migrates into a reservoir when it is water-wet. Thus, no brine is trapped and the connate or initial water saturation is much less than the irreducible water attained after oilflooding a previously waterflooded reservoir. The pore-level events which occur along the path to P_c^{max} during secondary drainage now reflect a mixed-wet porous medium.

Although the same capillary pressures are imposed, the endpoint saturations at P_c^{max} (points K on Figure 13 and P on Figure 14) are quite different. Figures 11a and 11b display the water/oil configurations prior to water snap-off which determine S_{wirr}. It is evident that Figure 11a (unstable lenses) leads to less irreducible water than Figure

11b (W/O emulsion films). As with residual oil saturation our model predicts irreducible water saturations larger than those found experimentally, again due to a lack of multiple interconnectedness among pores.

Discussion

Our proposed model of mixed-wettability has five important parameters which can be altered: maximum imposed capillary pressure, minimum imposed capillary pressure, disjoining pressure maximum, pore shape, and pore-size distribution. We consider briefly each in turn.

As the maximum imposed capillary pressure is increased, more thick protective water films spontaneously break to molecular films during pristine drainage. A larger fraction of the rock surface is then coated with asphaltenes and becomes oil wet. This effect is consistent with Salathiel's findings. As he decreased connate water saturation by increasing the imposed capillary pressure, his core samples displayed increased oil-wet behavior. More recently Jadhunandan and Morrow (1991) show experimentally that Berea sandstone changes from fairly strongly water-wet to mixed-wet in the presence of crude oil and brine when connate or initial water saturation is reduced by 10 %.

If all thick protective water films lining pore walls are broken under case 1 (unstable lenses), the porous medium exhibits an Amott-Harvey wetting index of approximately zero. Since there are no longer large water-wet pores, the capillary pressure drops precipitously from P_c^{max} to zero with little change in saturation upon imbibition. Upon secondary drainage, the capillary pressure still rises rapidly from P_c^{min} to zero with little change in saturation. These two results balance to give near neutral wettability. However, because the pore corners remain water-wet, the porous medium retains mixed-wettability character. Under case 2 (stable W/O emulsion films),

strongly oil-wet behavior (I_{wo} near -1) results because the stable W/O emulsion films span all pores except the very smallest ones. These films all refill with oil while P_c is negative giving greater oil-wet character. Again, mixed-wettability is retained because the pore corners remain water-wet.

When the P_c^{max} becomes infinite, S_{wc} approaches zero. All of the brine residing in pore corners is eliminated. In this instance all solid surfaces of the porous medium become oil-wet, and an I_{wo} of -1 results.

The minimum imposed capillary pressure is set to $-P_c^{max}$ for all calculations. A less negative P_c^{min} does not force all of the water/oil interfaces of the bridging-oil lenses to touch. A distribution of lenses in which the interfaces do and do not touch arises in the mixed-oil-wet pores. In case 1 not all of the oil lenses reach the unstable configuration. A mixture of broken and unbroken lenses at P_c^{min} gives capillary pressure curves which are a mixture of cases 1 and 2. The unbroken oil lenses refill in a manner analogous to the filling of the W/O emulsion films in case 2. In case 2, not all of the pores develop W/O emulsion films as P_c^{min} is made less negative. However, the capillary pressure curve is unaffected. A more negative P_c^{min} also has no effect, because there is very little additional oil to be recovered from the mixed-oil-wet pores in cases 1 and 2 .

Increasing the maximum in the solid/water/oil disjoining pressure curve (c.f. Figure 3) adds stability to the thick brine films coating pore walls. Thus, the critical capillary pressure, P_c^*, required to rupture thick films is increased following Eq. 5. As Π^{max} is increased, the porous medium portrays more water-wetting character. In the limit of a very large disjoining pressure maximum (e.g., case 3), a completely water-wet porous medium emerges. Thus, our picture explains mechanistically how surfaces may remain water-wet even when highly asphaltic oil is present.

Pore shape also has significant effect. For instance, in a concave pore, such as that with an eye-shaped cross-section in Figure 15a, the thinnest brine films line the

walls of the largest pores, whereas a convex pore shape (c.f., Figure 6) places the thinnest brine films in the smallest pores. Hence with eye-shaped pores, the largest oil-filled pores become mixed-oil-wet rather than the smallest oil-occupied pores. Remaining oil is still present as lenses or rivulets which bridge the corners of pores. Since oil traps only in the smaller volume water-wet pores, residual oil saturation is now lower.

A triangular pore (Figure 15b) allows all of the thick water films coating pore walls to break at the same capillary pressure. Results are then similar to those when the imposed capillary pressure is very large. In this instance, P_c^* corresponds exactly to Π^{max} because the walls of triangular pores are of zero curvature. Residual oil saturation is drastically lower than with either star or eye-shaped pores because all pores become mixed-oil-wet and undergo efficient drainage. As with both the star and eye-shaped pores, bridging-oil lenses are the source of remaining oil saturation. If bridging-oil lenses are unstable as in case 1, I_{wo} is approximately zero. For stable W/O emulsion films in case 2, strongly oil-wet behavior (I_{wo} near -1) results, but these pores retain some mixed-wettability character because the corners of the pore remain water-wet.

Morrow and Mason (1991) find that in perfectly wetting triangular capillaries the amount of trapped oil is reduced as the triangle becomes more irregular. Recall that the area of the largest circle that can be inscribed in a pore (displayed in all pore shapes of Figure 15) determines the amount trapped oil. The more irregular a triangle, the smaller the possible inscribed circle relative to the total triangle area. Asymmetry in convex (Figure 15c) or concave pore shapes also leads to less oil trapping and greater oil recovery.

The last pore shape considered is shown in Figure 15d. The walls of this star-shaped pore do not meet at a point. This shape arises when minerals deposit between grains (Salathiel, 1973). The corners are rounded and do not retain significant

amounts of brine at large imposed capillary pressures. Consequently, the entire pore wall becomes continuously oil-wet. If the imposed capillary pressure is again large, all pores are made oil-wet in this manner, the Amott-Harvey wetting index equals -1 indicative of strongly oil-wet conditions.

The fifth model parameter is the pore-size distribution. By decreasing the ratio of large-sized pores to small-sized pores, the amount of residual oil is reduced. Likewise, increasing the fraction of intermediate-sized mixed-oil-wet pores raises the amount of recoverable oil. Both of these changes shift I_{wo} toward more oil-wet conditions. When the smallest pores (representing micropores and pore throats) are trimmed from the distribution of pores sizes in Figure 12, small completely brine filled pores no longer exist and S_{wc} falls to zero. The shapes of the capillary-pressure curves (i.e., Figures 13 and 14) are not changed. They are merely shifted toward the left. Wettability indices are unaffected.

The pore surfaces considered in this work are smooth whereas roughness is the norm in reservoir media. Roughness causes an increasing difference in advancing and receding contact angles. Contact-angle hysteresis shifts fluid saturations during imbibition and drainage processes but does not lead to bridging oil-lenses as in Figure 10b and, therefore, is not the origin of the extended oil recovery found in mixed-wettability rock.

Thick wetting films make rough surfaces appear dramatically smoother when the average film thickness is larger than the distance between asperities (Robbins et al, 1991). These predictions are borne out by the experiments of Garoff et al (1989). Consequently, thick wetting films coating rough-curved pore surfaces smooth the film interface. The film thickness is then, in a large part, still determined by the underlying wall curvature. For our star-shaped pore model, the behavior of films on pores with rough walls mimics that of smooth tubes as long as the distance between surface

imperfections is small enough to permit smoothing of the liquid interface. The converse situation warrants investigation.

The collection of nonaxisymmetric capillaries model allows exploration of not only mixed-wettability behavior, but a wide variety of wetting behavior. Intermediate-wettability can be accommodated by altering the oil/water/solid disjoining pressure isotherm (c.f., Figure 3) to represent surfaces with finite contact angles. In fact, a surface with virtually any type of wettability can be modeled by adopting the appropriate disjoining pressure isotherm. We are also not limited to pore surfaces of uniform or symmetric wettability. One portion of the pore surface may be represented by a disjoining pressure isotherm for water-wetting minerals and another for oil-wetting minerals. The case of multiple occupancy of a single cornered pores by three phases (e.g., gas, oil, and water) appears even more intriguing and intricate.

Conclusions

Currently most models of flow in porous media are based on interconnected networks of pores whose typical shapes are either cylinders or unspecified. Although network models are very successful in explaining concepts such as relative permeability and trapping, they do not address the important issues of wettability and wettability alteration. At a fundamental level, nonaxisymmetric pore shapes and thin films are necessary to understand wettability.

We find that a delicate interplay between pore shape and thin-film chemistry and physics can predict mixed-wettability in porous rocks. In a distribution of star-shaped pores, the largest pores are prevented from becoming mixed-oil-wet because their pore walls are protected by thick continuous water films. These films prohibit asphaltene adsorption and subsequent alteration in the wettability state of the pore surface. Conversely, ultrathin, molecular films form on the walls of intermediate-sized

star-shaped pores during pristine drainage. These films permit irreversible asphaltene adsorption, and subsequently these pores become mixed-oil-wet. The smallest pores which are never entered by oil remain water-wet.

Our proposed suite of pore-level events correctly describes the essential observations associated with mixed-wettability reservoir rocks. Capillary pressure curves mimic those generated experimentally in the laboratory. Foremost, a significant reduction, compared to water-wet rock, in residual oil saturation is predicted. The correct trends of wettability index are found in that lower initial brine saturations lead to greater oil-wettability.

Remaining oil saturation, the long period of oil production, and high-efficiency waterfloods of mixed-wettability porous media are attributed to the formation of thick oil lenses or rivulets which span the corners of pores in addition to oil films adhering to pore walls. Oil drainage is consequently very slow. With star-shaped pores these lenses or rivulets reside in pores of intermediate size. The notion of contact angle-pinning allows development of the bridging oil lenses.

Because the largest pores remain water-wet, oil snaps off and is trapped in a manner identical to the creation residual oil in completely water-wetting porous media. Irreducible snapped-off water is also formed during secondary drainage because brine is trapped in mixed-oil-wet pores in a fashion similar to the creation of residual oil in water-wet porous media. In contrast to water-wet systems, connate and irreducible water saturation are shown to be quite different in mixed-wettability systems. Since wettability states undergo change at or near S_{wc}, there is a corresponding change in pore-level mechanisms for mixed-wettability systems. Irreducible water, consistent with experimental observations, is predicted to be greater for mixed-wettability systems than for water-wetting systems due to the formation of discontinuous trapped water.

Acknowledgement

This work was supported by the U.S. Department of Energy under contract No. DC03-76F00098 to the Lawrence Berkeley Laboratory of the University of California.

Notation

a= radius of circle which can be inscribed in pore, m

A_i = cross sectional area, m^2

d_i= bead diameter, m

h = equilibrium film thickness, m

h_i = equilibrium film thickness overlaying a bead of diameter d_i, m

h_p= range of film thickness where disjoining pressure is relevant, m

I_i=wettability index

I_{wo}= Amott-Harvey wettability index

P_c = capillary pressure, difference in oil and water phase pressure, N/m^2

P_{nw} = nonwetting phase pressure, N/m^2

P_w = wetting phase pressure, N/m^2

r_1, r_2 = principal radii of curvature, m

S_i = phase saturation, ratio of the area occupied by a phase to total area of the system

Subscripts and Superscripts

* = critical value for thick film rupture

e = entry for a particular size pore

max = maximum

m = mean

o = oil

or = residual oil

t = total

w = water

wc = connate water

wirr = irreducible water

Greek letters

Π = disjoining pressure, Pa

σ = interfacial tension, N/m

θ = equilibrium contact angle measured through the aqueous phase

ΔS_{os}=saturation change during secondary drainage

ΔS_{ws}=saturation change during spontaneous imbibition

ΔS_{wt}=overall saturation change during imbibition

ξ = dummy variable of integration, m

Literature cited

Amott, E., "Observations Relating to the Wettability of Porous Rock," Trans AIME, 216, 156-162 (1959).

Buckley, J. S., K. Takamura, and N. R. Morrow, "Influence of Electrical Surface Charges on the Wetting Properties of Crude Oil," Soc. Pet. Eng. Res. Eng., 4(3), 332-340 (1989).

Buckley, J. S., and N. R. Morrow, "Characterization of Crude-Oil Wetting Behavior by Adhesion Tests," SPE 20263, presented at SPE/DOE Symposium on Enhanced Oil Recovery, Tulsa, OK (April 1990).

Callaghan, I. C. and K. W. Baldry, "The Thickness of Aqueous Wetting Films on Silica," in Wetting Spreading and Adhesion, J. F. Padday ed., Academic Press, London, Ch.7 161-181 (1978).

Chambers, K. T. and C. J. Radke, "Capillary Phenomena in Foam Flow Through Porous Media," in Interfacial Phenomena in Petroleum Recovery, N. R. Morrow ed., Marcel Dekker Inc, New York, Ch.6 191-255 (1991).

Chung, F., Sarathi, P., and Jones, R., "Modeling of Asphaltene and Wax Precipitation," NIPER-498, DOE Topical Report, Bartlesville, OK (January,1991).

Clementz, D. M., "Interaction of Petroleum Heavy Ends with Montmorillonite," Clays and Clay Min., 24, 312-319 (1976).

Clementz, D. M., "Alteration of Rock Properties by Adsorption of Petroleum Heavy Ends: Implications for Enhanced Oil Recovery," SPE 10683, presented at SPE/DOE Joint Symposium on Enhanced Oil Recovery, Tulsa, OK (April, 1982).

Craig, F. F. Jr., The Reservoir Engineering Aspects of Waterflooding, Society of Petroleum Engineers of AIME, New York, 12-19 (1971).

Cuiec, L. E., "Evaluation of Reservoir Wettability and Its Effect on Oil Recovery," in Interfacial Phenomena in Petroleum Recovery, N. R. Morrow ed., Marcel Dekker Inc, New York, Ch.9 319-373 (1991).

Derjaguin, B. V. and E. V. Obukhov, "Anomalien dünner Flüssigkeitsschichten III," Acta Physicochim. URSS, 5(1), 1-22 (1936).

Derjaguin, B. V. and M. M. Kussakov, "Anomalous Properties of Thin Polymolecular Films V.," Acta Physicochim. URSS, 10(1), 25-44 (1939a).

Derjaguin, B. V. and M. M. Kussakov, "Anomalous Properties of Thin Polymolecular Films V.," Acta Physicochim. URSS, 10(2), 153-174 (1939b).

Derjaguin, B. V., Z. M. Zorin, N. V. Churaev, and V. A. Shishin, "Examination of Thin Layers on Various Solid Substrates," in Wetting, Spreading and Adhesion, J. F. Padday ed., Academic Press, London, Ch. 9 201-212 (1978).

Derjaguin, B. V., N. V. Churaev, and V. M. Muller, Surface Forces, Consultants Bureau, New York, 25-52 327-367 (1987).

Dubey, S. T. and M. H. Waxman, "Asphaltene Adsorption and Desorption From Mineral Surfaces," Soc. Pet. Eng. Res. Eng., 6(3), 389-395 (1991).

Fassi-Fihri, O., M. Robin, E. Rosenberg, "Wettability Studies at the Pore Level: A New Approach by the Use of Cryo-Scanning Electron Microscopy," SPE 22596, presented at SPE Annual Tech. Conf., Dallas, TX (October, 1991).

Garoff, S., E. B. Sirota, S. K. Sinha, and H. B. Stanley, "The Effects of Substrate Roughness on Ultrathin Water Films," J. Chem. Phys., 90(12), 7505-7515 (1989).

Hall, A. C., S. H. Collins, and J. C. Melrose, "Stability of Aqueous Wetting Films in Athabasca Tar Sands," Soc. Pet. Eng. J., 23(2), 249-258 (1983).

Hirasaki, G. J., J. A. Rohan, S. T. Dubey, "Wettability Evaluation During Restored-State Core Analysis," SPE 20506, presented at SPE Annual Tech. Conf., New Orleans, LA (September 1990).

Hirasaki G. J., "Wettability: Fundamentals and Surface Forces," Soc. Pet. Eng. Form. Eval., 6(2), 217-226 (1991).

Jadhunandan, P. P. and N. R. Morrow, "Effect of Wettability on Waterflood Recovery for Crude-Oil/Brine/Rock Systems, SPE 22597, presented at SPE Annual Tech. Conf., Dallas, TX (October, 1991).

Kovscek, A. R., PhD Dissertation, University of California, Berkeley, in progress (1992).

Mayer, R. P. and R. A. Stowe, "Mercury Porosimetry--Breakthrough Pressure for Penetration between Packed Spheres," J. Coll. Interf. Sci., 20, 893-911 (1965)

Melrose, J. C., "Interpretation of Mixed Wettability States in Reservoir Rocks," SPE 10971, presented at SPE Fall Tech. Conf., New Orleans, LA (September 1982).

Mohanty, K. K., H. T. Davis, and L. E. Scriven, "Physics of Oil Entrapment in Water-Wet Rock," Soc. Pet. Eng. Res. Eng., 2(1), 113-128 (1987).

Mohanty, K. K. and A. E. Miller, "Factors Influences Unsteady Relative Permeability of a Mixed-Wet Reservoir Rock," Soc. Pet. Eng. Form. Eval, 6(3), 349-358 (1991).

Morrow, N.R. and C. C. Harris, "Capillary Equilibrium in Porous Materials," Soc. Pet. Eng J., 5(1), 35-24 (1965).

Morrow, N. R., H. T. Lim, and J. S. Ward, "Effect of Crude-Oil Induced Wettability Changes on Oil Recovery," Soc. Pet. Eng. Form. Eval., 1(1), 89-103 (1986).

Morrow, N. R., "Wettability and Its Effect on Oil Recovery," J. Pet. Tech., 42(12), 1476-1484 (1990).

Morrow, N. R., "Introduction to Interfacial Phenomena in Oil Recovery," in Interfacial Phenomena in Petroleum Recovery, N. R. Morrow ed., Marcel Dekker Inc, New York, Ch. 1 1-22 (1991).

Morrow, N. R. and G. Mason, "Capillary Behavior of a Perfectly Wetting Liquid in Irregular Triangular Tubes," J. Coll. Interf. Sci, 141(1), 262-274 (1991) .

Ransohoff, T. C., P. A. Gauglitz, and C. J. Radke, "Snap-Off of Gas Bubbles in Smoothly Constricted Noncircular Capillaries," AIChE Journal, 33(5), 753-765 (1987).

Robbins, M. O., D. Andelman, J. F. Joanny, "Thin Liquid Films on Rough Heterogeneous Solids," Phys. Rev. A, 43(8), 4344-4354 (1991).

Roof, J. G., "Snap-Off of Oil Droplets in Water-Wet Pores," Soc. Pet. Eng. J., 10(1), 85-90 (1970).

Salathiel, R. A., "Oil Recovery by Surface Film Drainage in Mixed-Wettability Rocks," J. Pet. Tech., 25(10), 1216-1224 (1973).

Sharma, M. M. and R. W. Wunderlich, "The Alteration of Rock Properties Due to Interactions With Drilling-Fluid Components," J. Pet. Science & Eng., 1, 127-43 (1987).

Slobod, R. L., A. Chambers, and W. L. Prehn Jr., "Use of Centrifuge for Determining Connate Water, Residual Oil, and Capillary Pressure Curves of Small Core Samples," Trans AIME, 192, 127-134 (1951).

Wardlaw, N. C., Y. Li ., and D. Forbes, "Pore-Throat Size Correlation from Capillary Pressure Curves," Transport in Porous Media, 2, 597-614 (1987).

Wong, H., S. Morris, and C. J. Radke, "Three Dimensional Menisci in Polygonal Capillaries," J. Coll. Inter. Sci, 148(2), 317-336 (1992).

Table 1: Amott-Harvey Indices and Residual Oil Saturations for Water-Wet and Mixed-Wet Porous Media.

case	$\frac{a_m \Pi^{max}}{\sigma}$	I_{ow}	S_{or}
1: unstable lenses	18	0.36	0.35
2: stable W/O emulsion films	18	-0.18	0.35
3: water-wet	180	1.0	0.54

Figure Captions

Figure 1: Mechanisms of oil surface drainage in mixed-wettability systems (after Salathiel, 1973).

Figure 2: Schematic diagram of an apparatus for measuring thin-film forces in solid/liquid systems (after Derjaguin et al, 1978).

Figure 3: Schematic disjoining pressure isotherm for wetting films on solids.

Figure 4: Wetting films covering sand grains.

Figure 5: Typical experimental capillary pressure versus aqueous phase saturation curves (a) water-wet 48-60 mesh glass beads (data of Morrow and Harris, 1965) (b) weakly mixed-wet sandstone (data of Mohanty and Miller, 1991).

Figure 6: Cross section of a translationally invariant star-shaped pore.

Figure 7: Water-wet pore just after oil entry.

Figure 8 Schematic of a mixed-oil-wet pore illustrating the location of asphaltene deposition and the coexistence of oil-wet and water-wet regions within a single pore.

Figure 9: Imbibition processes in a water-wet pore.

Figure 10 Imbibition processes in a mixed-oil-wet pore (a) spontaneous imbibition (b) just after brine entry during forced imbibition.

Figure 11: Secondary drainage in mixed-oil-wet pores (a) case 1, unstable lenses (b) case 2, stable W/O emulsion films.

Figure 12: Discrete size distribution of star-shaped pores.

Figure 13: Capillary pressure versus aqueous phase saturation, case 1 unstable lenses.

Figure 14: Capillary pressure versus aqueous phase saturation, case 2 stable W/O emulsion films.

Figure 15: Alternative cross-sectional pore shapes (a) eye-shaped (b) irregular-triangle (c) irregular-star (d) star-shaped with mineral deposits in pore corners.

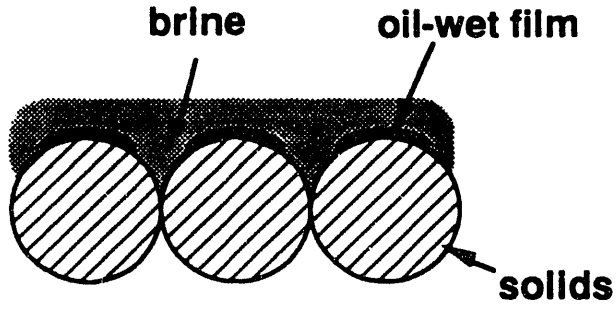

Figure 1:

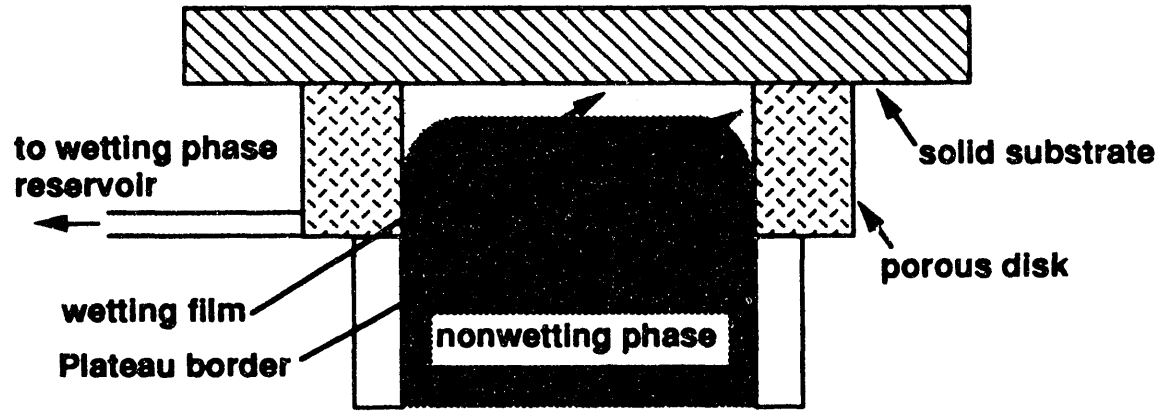
to wetting phase
reservoir
solid substrate
porous disk
wetting film
Plateau border
nonwetting phase

Figure 2:

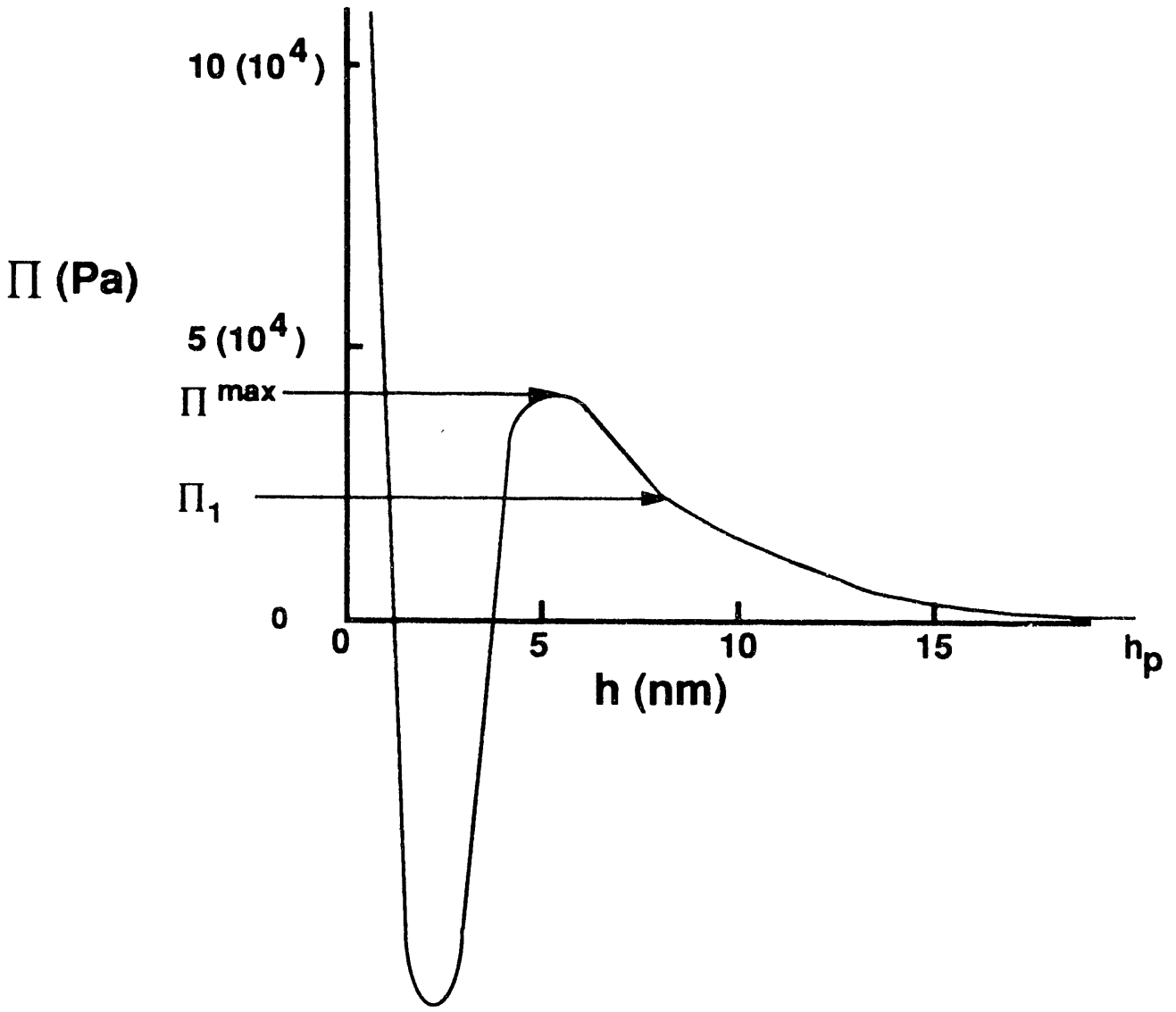

Figure 3:

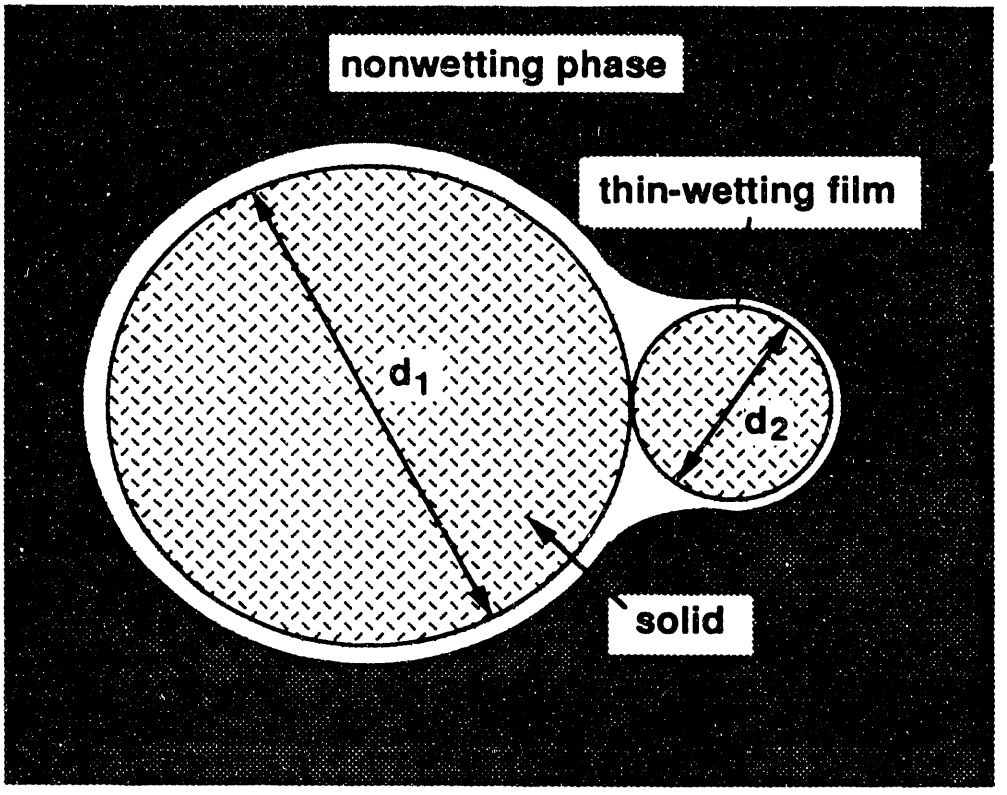

Figure 4

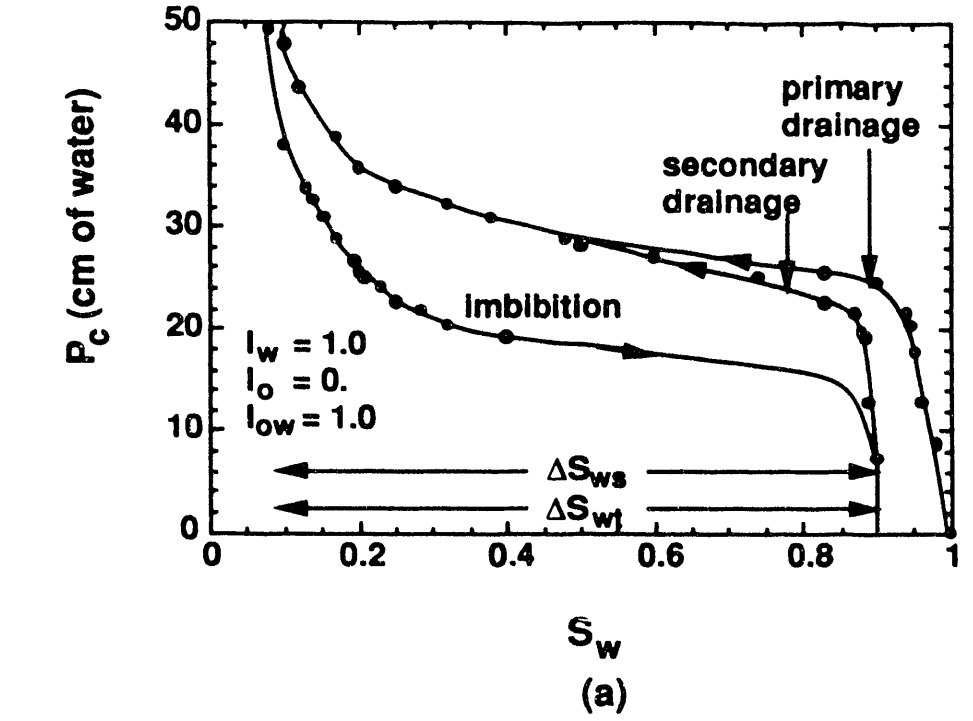
50
40
30
20
10
0
0
0.2
0.4
0.6
0.8
1
P_c (cm of water)
primary drainage
secondary drainage
imbibition
I_w = 1.0
I_o = 0.
I_{ow} = 1.0
ΔS_{ws}
ΔS_{wt}
S_w
(a)

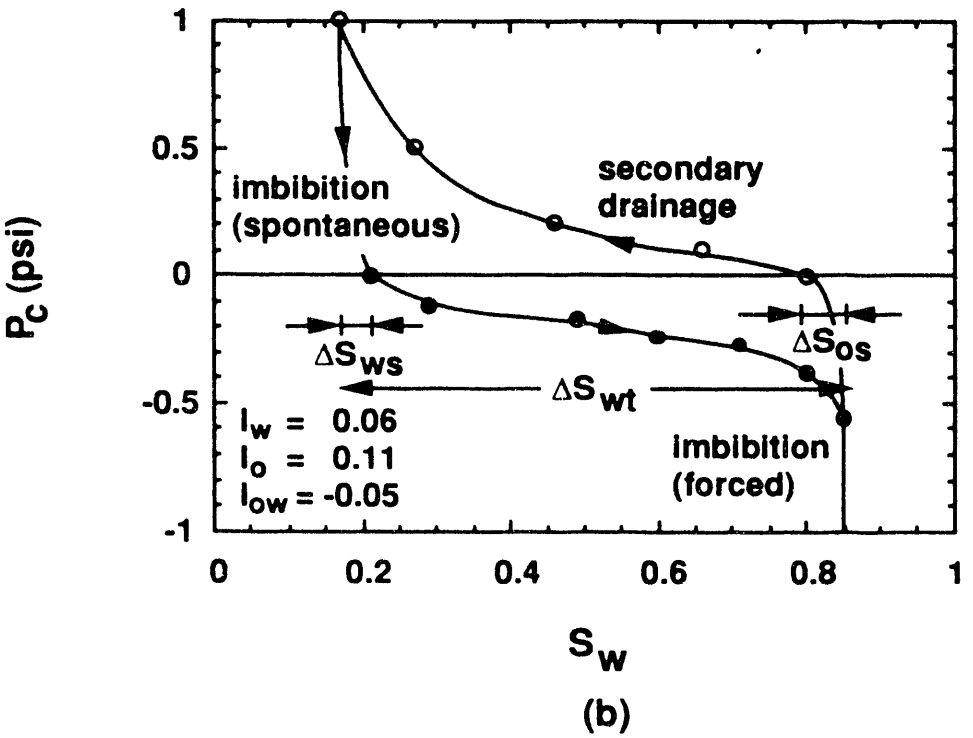
1
0.5
0
-0.5
-1
0
0.2
0.4
0.6
0.8
1
P_c (psi)
imbibition (spontaneous)
secondary drainage
ΔS_{ws}
ΔS_{wt}
ΔS_{os}
I_w = 0.06
I_o = 0.11
I_{ow} = -0.05
imbibition (forced)
S_w
(b)

Figure 5

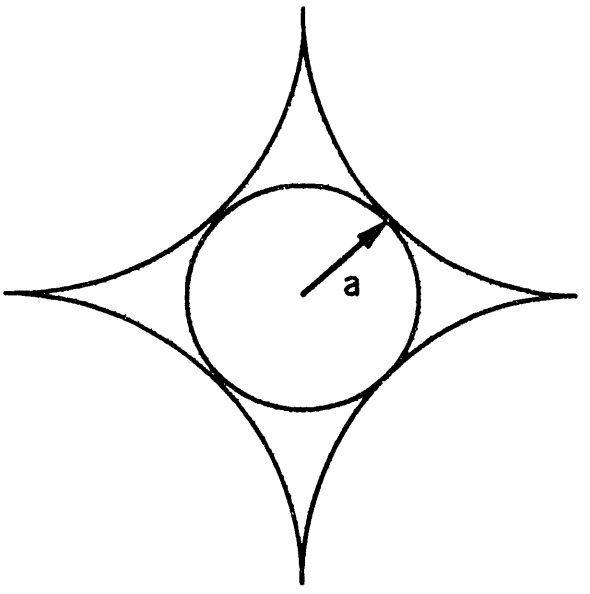

Figure 6

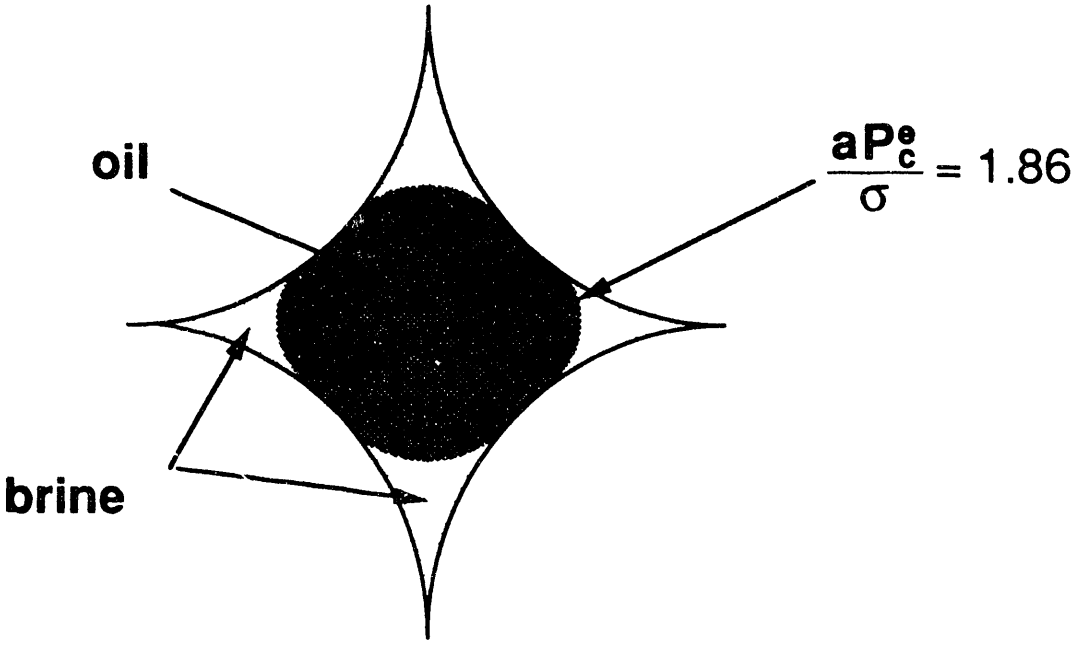

Figure 7

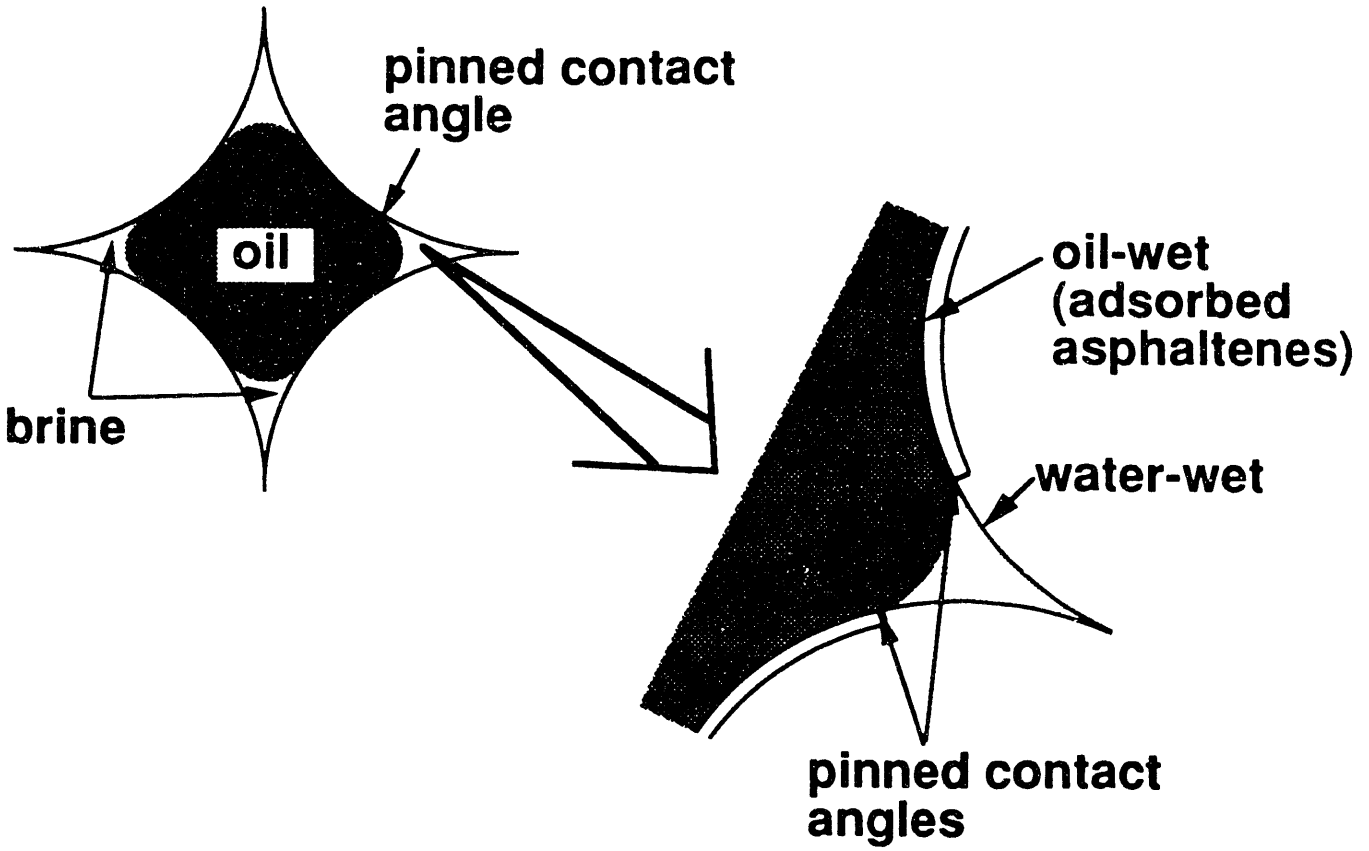
pinned contact
angle
oil
brine
oil-wet
(adsorbed
asphaltenes)
water-wet
pinned contact
angles

Figure 8

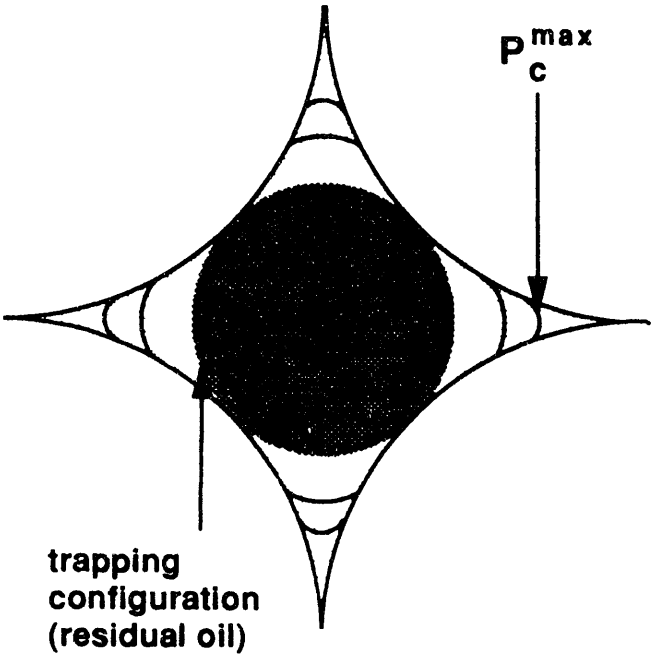

water-wet pore

Figure 9

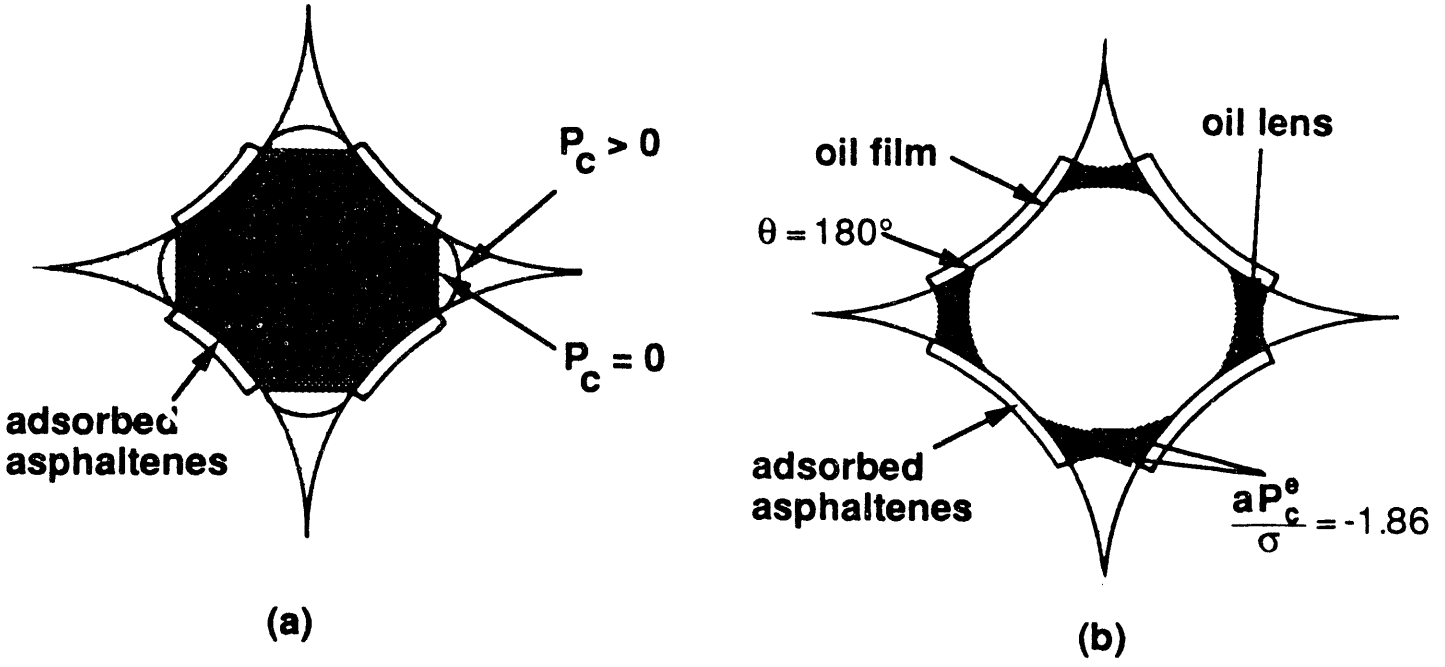
$P_c > 0$
$P_c = 0$
adsorbed asphaltenes
(a)
oil film
oil lens
$\theta = 180°$
adsorbed asphaltenes
$\frac{aP_c^e}{\sigma} = -1.86$
(b)

Figure 10

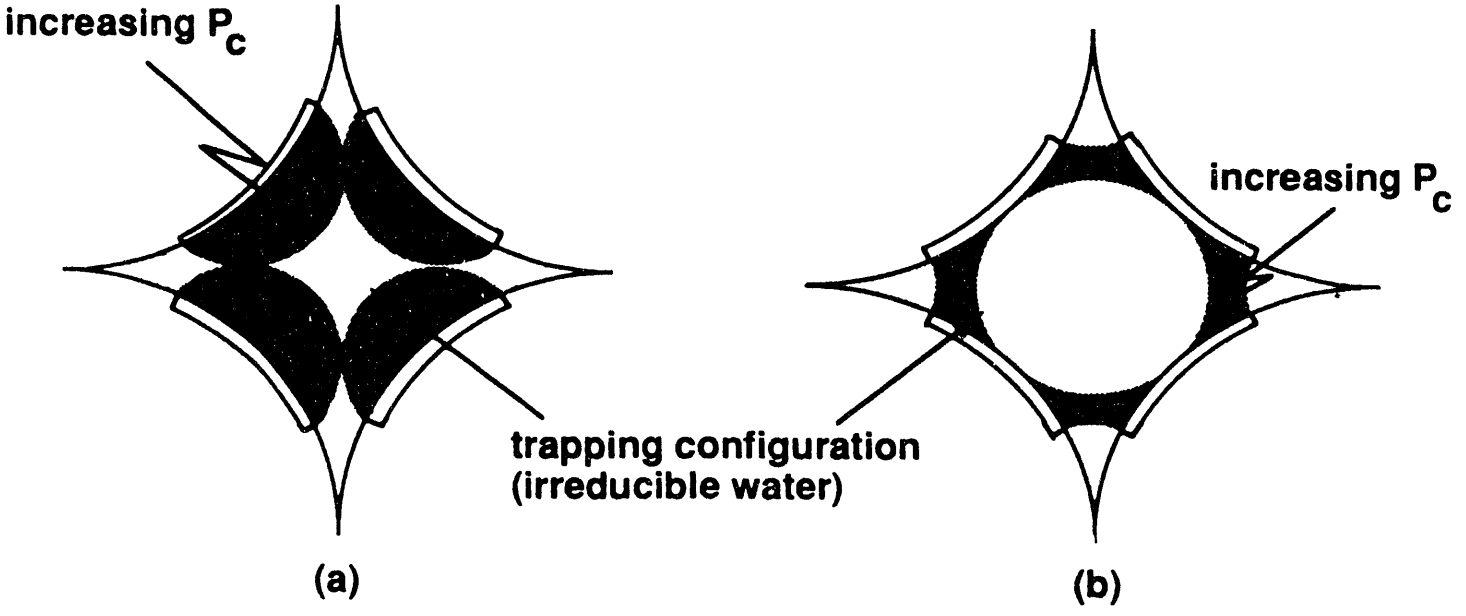
increasing P_c
increasing P_c
trapping configuration
(irreducible water)
(a)
(b)

Figure11

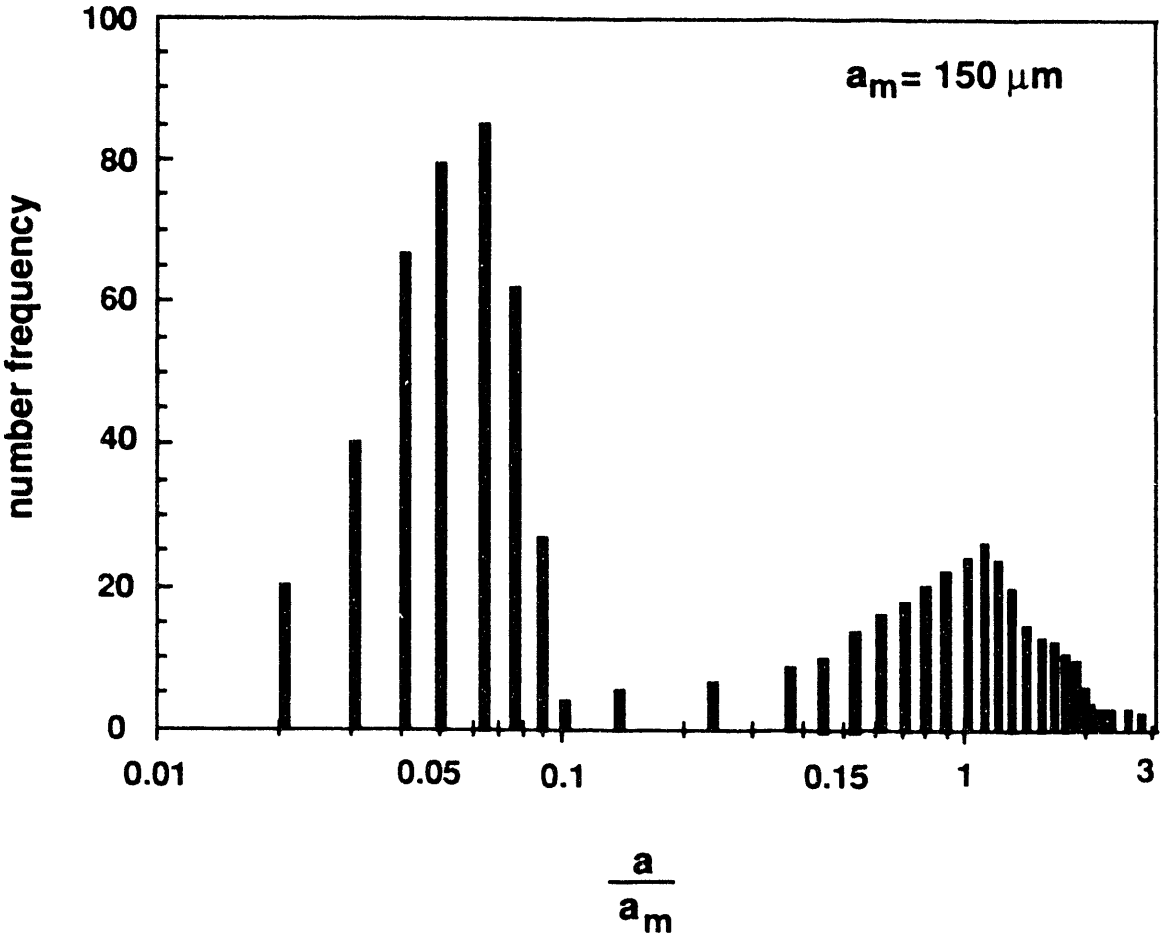
100
80
60
40
20
0
number frequency
a_m= 150 μm
0.01
0.05
0.1
0.15
1
3
$\frac{a}{a_m}$

Figure 12

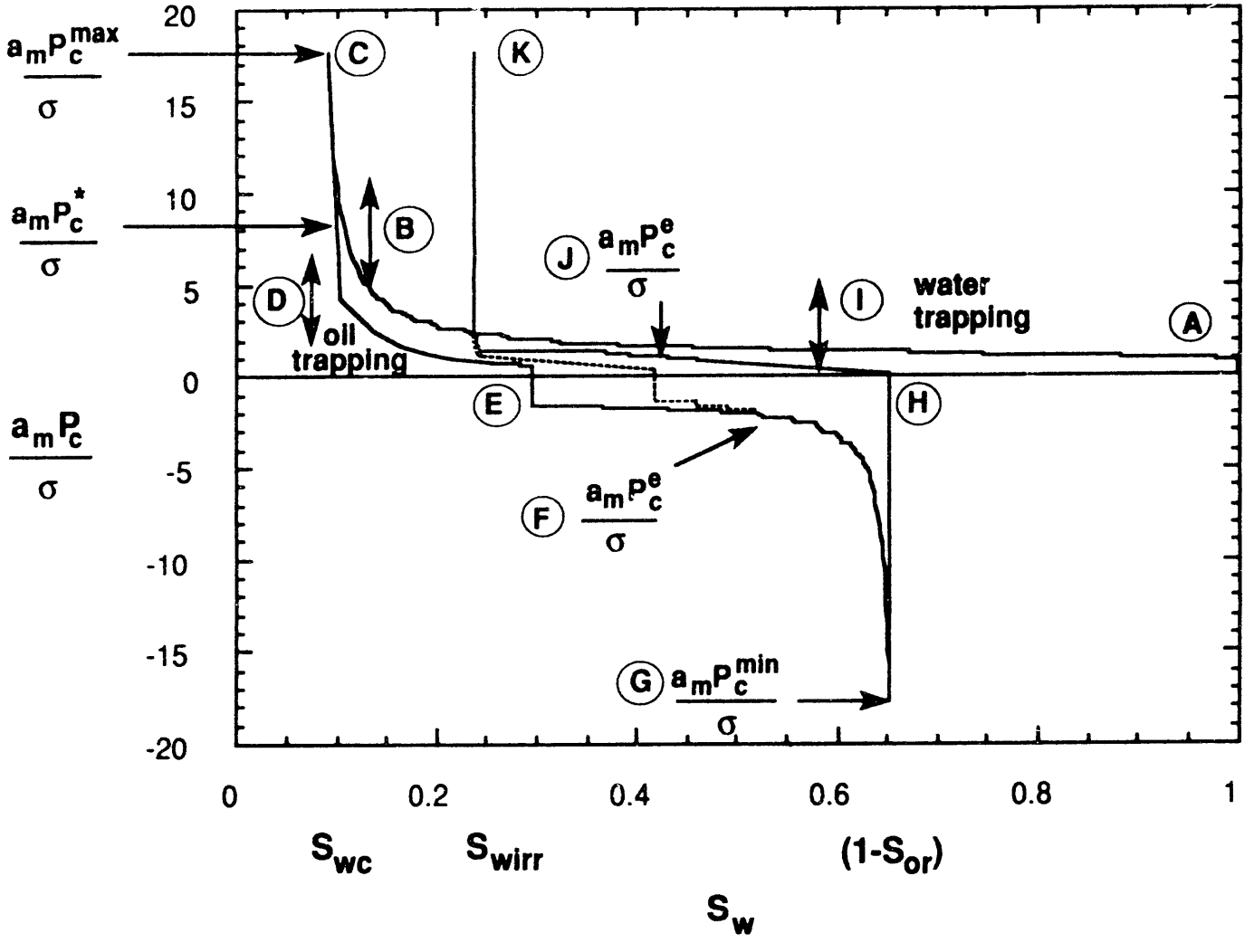
20
15
10
5
0
-5
-10
-15
-20
$a_m P_c^{max}/\sigma$
$a_m P_c^*/\sigma$
$a_m P_c/\sigma$
C
K
B
D
oil trapping
J
$a_m P_c^e/\sigma$
I
water trapping
A
E
H
F
$a_m P_c^e/\sigma$
G
$a_m P_c^{min}/\sigma$
0
0.2
0.4
0.6
0.8
1
S_{wc}
S_{wirr}
$(1-S_{or})$
S_w

Figure 13

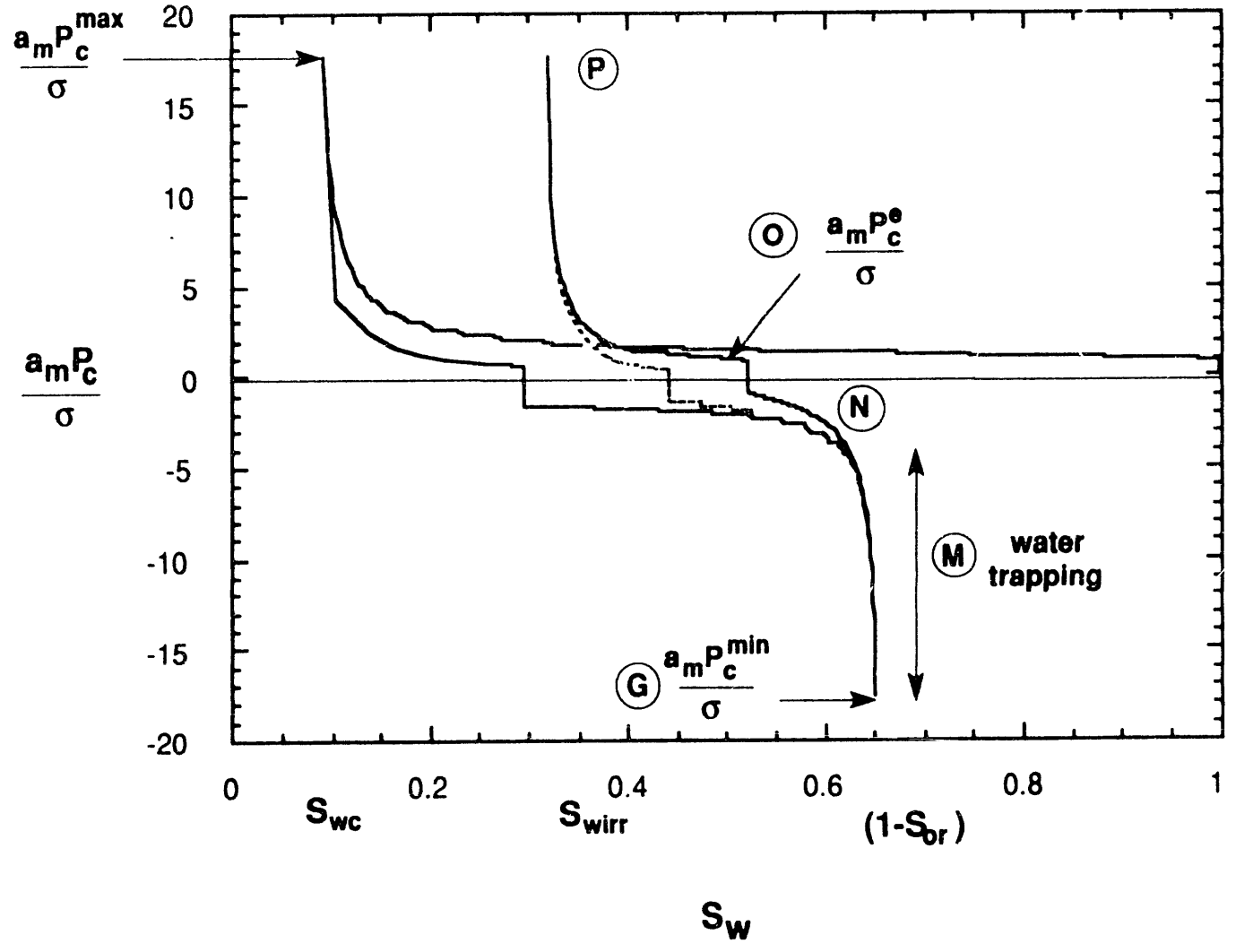
$a_m P_c^{max}/\sigma$
20
15
10
5
0
-5
-10
-15
-20
$a_m P_c/\sigma$
P
O
$a_m P_c^e/\sigma$
N
M
water trapping
G
$a_m P_c^{min}/\sigma$
0
0.2
0.4
0.6
0.8
1
S_{wc}
S_{wirr}
$(1-S_{or})$
S_w

Figure 14

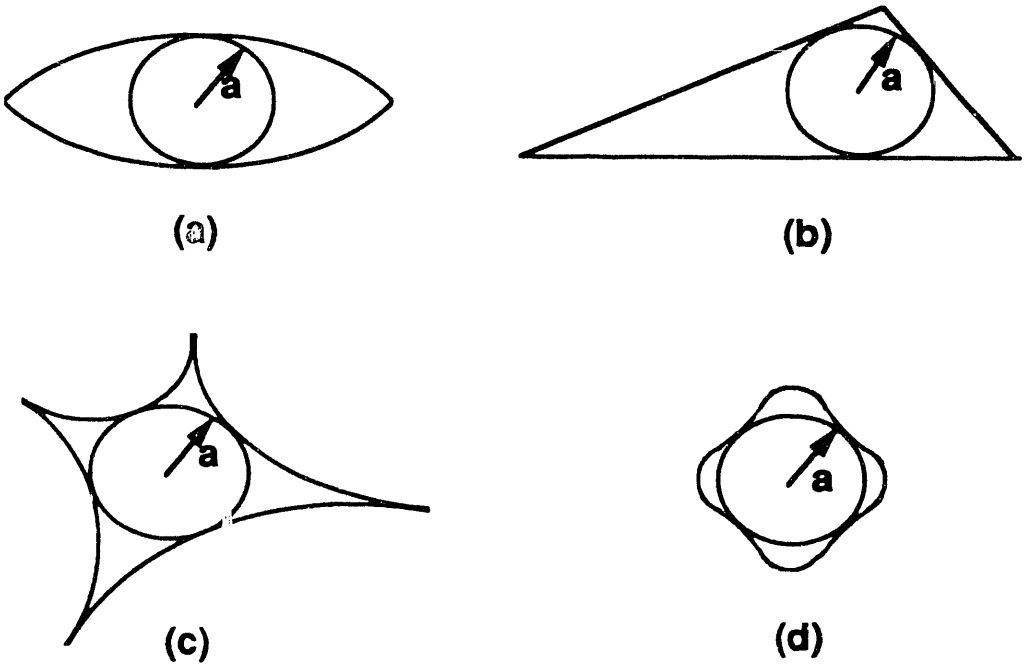

Figure 15

*U.S.GPO:1992-661-026/60047

END

DATE
FILMED
10/14/92